Journal of Materials Chemistry A

Accepted Manuscript

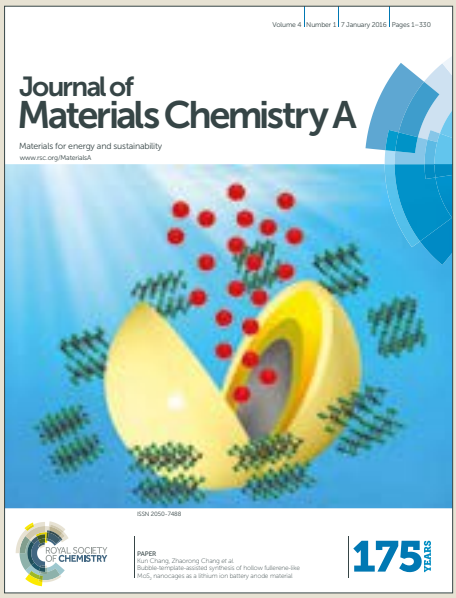

ROYAL SOCIETY OF CHEMISTRY

rsc.li/materials-a

View Article Online
DOI: 10.1039/C8TA00879E

Journal Name

ARTICLE

Enhanced Cycling Stability of Li-O_2 Batteries by Using a Polyurethane/SiO_2/Glass Fiber Nanocomposite Separator

Kun Luo,*[a] Guangbin Zhu,[b] Yuzhen Zhao,[b] Zhihong Luo,*[b] Xiaoteng Liu,[d] Kui Zhang,[c] Yali Li[a] and Keith Scott[c]

A considerable improvement on the cyclic performance of aprotic Li-O_2 batteries was achieved by using a polyurethane/SiO_2 gel nanoparticles/glass fiber (PU/SiO_2/GF) nanocomposite separator, where a persistent capability of 1000 mAh g^{-1} was maintained for at least 300 charge/discharge cycles in the DMSO electrolyte with 1 M $LiClO_4$ and 0.05 M LiI. In comparison, the cell with the conventional GF separator in the same experimental setup only run for 60 cycles. SEM, XRD and FT-IR analyses indicate that the corrosion and dendritic growth of the Li anode were significantly inhibited during the charge/discharge cycling, and the eventual failure of the Li-O_2 batteries was attributed to the cathode passivation caused by the accumulation of discharge product, which blocked the transfer of oxygen and electrolyte to the MWNTs cathode.

Received 00th January 20xx,
Accepted 00th January 20xx

DOI: 10.1039/x0xx00000x

www.rsc.org/MaterialsA

Introduction

Aprotic lithium-oxygen (Li-O_2) batteries have recently received considerable attention for their ultrahigh theoretical energy density ($\approx$3600 Wh kg^{-1}) compared to Li-ion batteries.[1] Advances have been made on overcoming the sluggish charge/discharge kinetics of the batteries by using appropriate catalysts and variant porous cathodes.[2-4] However, challenges are still present on the limited cycle life of aprotic Li-O_2 batteries,[1] which arise either from the passivation of porous cathodes or the corrosion of Li anode.

Several strategies have been developed to avoid the complete covering of the porous cathode by the insulating Li_2O_2 and other byproducts, which include: (1) Using soluble catalysts or redox mediators (RMs), including LiI, 2,2,6,6-tetramethylpiperidinyloxyl (TEMPO), tetrathiafulvalene (TTF) and phthalocyanine (FePc) etc.,[5-8] to promote the decomposition of discharge products in electrolytes; (2) Controlling over the morphology of discharge products to preserve the conductivity of porous cathodes, by using high donor number (DN) solvents, weakening the interaction between cathode and discharge products or discharging at low current density;[9-11] (3) Alternating the battery reaction chemistry to reduce the charge overpotential and retard the accumulation of discharge products, such as using LiO_2 or LiOH as discharge product or introducing H_2O into the battery electrolyte.[12-14]

Moreover, the protection of Li anodes has also attracted contemporary interest.[15,16] It is accepted that the solid electrolyte interface (SEI) enables the active Li metal serve as anode in aprotic electrolytes with a voltage window of more than 4 V. However, in Li-O_2 batteries the SEI layer on the Li surface is not quite stable during charge/discharge cycling due to the obvious interface and volume fluctuations, which frequently result in dendritic growth of Li crystals, and then possibly give rise to internal short circuit and thermal runaway.[17] The corrosion by the crossover species, including the dissolved O_2, discharge intermediates (O_2^- and O_2^{2-}), moisture, cleavage products of binders and electrolytes as well as RMs,[18-21] also challenge the durability of Li anodes. Zhou et al. stressed that the Li corrosion is more crucial for the long-term cycling stability of Li-O_2 batteries.[17]

To solve the problem, Li-Si, $LiFePO_4$ and Li alloy were reported to substitute Li plates,[7, 22-23] which apparently prolonged the cell cycling life at the price of capacity loss. Constructing artificial layers on the surface of Li anodes was also adapted, by means of the interfacial reaction with In^{3+} or fluoroethylene carbonate (FEC);[24,25] or by the direct coating of Al_2O_3/PVdF-HFP or AlF_3/PEDOT-co-PEG composites,[26,27] which alleviated the deterioration of Li anodes. However, no indication shows that these protective layers can withstand the significant morphology and volume variation of Li surface during long-term charge/discharge cycling. In this context,

[a] School of Materials Science and Engineering, Changzhou University, Changzhou 213164, P R China. Email: luokun998@gmail.com
[b] College of Materials Science and Engineering, Guilin University of Technology, Guilin 541004, P R China. Email:luozhihong613@glut.edu.cn
[c] School of Engineering, Newcastle University, Newcastle-upon-Tyne, NE1 7RU, UK
[d] Department of Mechanical and Construction Engineering, Northumbria University, Newcastle- upon-Tyne, NE1 8ST, UK

† Electronic Supplementary Information (ESI) available: [details of any supplementary information available should be included here]. See DOI: 10.1039/x0xx00000x

View Article Online
DOI: 10.1039/C8TA00879E

some turned to develop poreless, air-impermeable and waterproof separators. Kim [28] and Xu [29] utilized the modified polyurethane and Nafion films as separators, and the cyclic performance of Li-O_2 batteries was effectively improved, however, the internal resistance was largely increased as well, owing to the poor ionic conductivity of these separators. Herein, a polyurethane/SiO_2 gel nanoparticles/glass fiber (PU/SiO_2/GF) nanocomposite separator was designed and fabricated for aprotic Li-O_2 batteries, where the SiO_2 gel nanoparticles filled GF served as the supporting framework and Li^+ conductor, and the outer PU coating played as the air-impermeable and waterproof separator. The cycling performance of the Li-O_2 batteries with the PU/SiO_2/GF nanocomposite separator was massively improved in comparison to those with conventional GF separators, where the dendritic growth and the corrosion of Li were also effectively inhibited.

Experimental

Materials

Multi-walled carbon nanotubes (MWNTs, d=10±1 nm, L= 3-6 μm, Sigma-Aldrich), polyurethane (PU, Bayer), tetraethoxysilane (AR, Sinopharm), ammonia hydroxide (25 wt.%, Sinopharm), ethanol (AR, Sinopharm), carbon paper (TORAY, TGP-H-060), DME (anhydrous, 99.5%, Sigma-Aldrich) and borosilicate glass fiber filter paper (GF, d=18 mm, Whatman) were used directly as received. Prior to use, dimethyl sulfoxide (DMSO, 99.9%, Sigma-Aldrich) and propylene carbonate (PC, 99.7%, Sigma-Aldrich) were dehydrated with activated 4Å molecular sieves, and lithium perchlorate ($LiClO_4$, 99.99%, Sigma-Aldrich) and lithium iodide (LiI, 99.9%, Sigma-Aldrich) were dried at 160 ℃ and 200 ℃ in a vacuum oven for 12 h, respectively. Li plates (Shenzhen Poxon Machinery Technology Co. Ltd.) were immersed in a PC solution containing 0.1 M $LiClO_4$ for at least two days.

Preparation of the PU/SiO_2/GF nanocomposite separator

SiO_2 gel nanoparticles were synthesized by the following procedure:[30] ethanol (84 mL), ammonia hydroxide (25.5 mL) and deionized water (50 mL) were added in sequence and mixed in a beaker, and then 20 mL of tetraethoxysilane were injected dropwise followed with magnetic stirring for 8 h, resulted in white precipitates on the bottom of the beaker. The precipitates were separated and rinsed with ethanol for three times by centrifuging (3000 r min^{-1}), and then was dried at 120 °C for 4 h, led to the SiO_2 gel nanoparticles.

1.0 g of PU powders were dispersed into 10 mL NMP with magnetic stirring, and then 0.2 g of PC was injected into the NMP suspension. The mixture was stirred for 30 min, and then stood over 24 h, led to the PU solution after stirring.

2.5 g of the SiO_2 gel nanoparticles were dispersed into 10 mL deionized water by ultrasonic stirring, and then a GF separator was immersed in the as-prepared SiO_2 suspension for 30 s, which was lifted up and dried at 120 °C for 1 h. This operation was repeated for three times, resulted in the filling of SiO_2 gel nanoparticles into the GF separator (i.e. SiO_2/GF). After that, the SiO_2/GF was brushed with PU solution, and then was dried at 120 °C for 1 h. This procedure was also repeated for three times, led to the PU/SiO_2/GF nanocomposite separator at last.

Assembly and testing of Li-O_2 batteries

3 mg of MWNTs were dispersed in 10 mL ethanol by ultrasonic stirring, and the slurry was sprayed onto carbon paper with a loading of 0.1 mg cm^{-2}, which was dried in a vacuum oven at 60 °C overnight. The carbon paper with MWNTs was cut to fit the holed CR2302 coin cell, which served as the cathodes in the aprotic Li-O_2 batteries.

The coin cells were assembled in an argon-filled glovebox (Mikrouna Co., Ltd., H_2O < 0.1 ppm, O_2 < 0.1 ppm), which were tested by a Battery Testing System (CT-3008W-5V10mA, Neware Technology Co. Ltd., China) in a home-made gas proof container with pure oxygen atmosphere (≥99.9%, 1.1 atm). In long-term cycling experiments, the cutoff potentials were set up at 2.0 V and 4.5 V with the current density of 1 A g^{-1} based on the loading mass of MWNTs, and the charge/discharge capacity was settled at 1000 mAh g^{-1}. The coin cells were disassembled in the glove box, and the electrodes and separators after use were rinsed with DME and dried in pure argon at room temperature before further characterization.

Characterizations

The morphology and structure of the cathodes, anodes and separators were characterized by a field-emission scanning electron microscope (SEM, S-4800, Hitachi) and an X-ray diffractometer (XRD, X'Pert PRO). The composition of the separators was also investigated by the attenuated total reflectance of Fourier transform infrared spectroscopy (ATR-FTIR, IRTracer-100, Shimadzu).

The ionic conductivity (σ) of the separators was measured by an electrochemical workstation (CHI 750E, CH Instruments) in the coin cells with a symmetric sandwich structure, i.e. two stainless steel (SS) electrodes were placed at the both sides of the separator (SS/separator/SS), where 1 M $LiClO_4$ in DMSO was injected as the electrolyte. The conductivity of the separator was estimated by the following equation:

$$\sigma = d/R_b S \quad (1)$$

where d is the thickness of the tested separator, R_b is the measured electrical resistance, and $S=\pi r^2$ is the geometric area of the SS electrode.

Results and discussion

Structure of the PU/SiO_2/GF nanocomposite separator

The morphological evolution from the GF separator to the PU/SiO_2/GF nanocomposite separator is characterized by SEM. As shown in Fig.1a, enormous large pores constructed by the nonwoven glass fibers are present in the conventional GF, which only serves to segregate the MWNTs cathode and Li anode by its thickness. Fig.1b illustrates the SEM micrograph of the GF separator filled with SiO_2 gel nanoparticles after dipping in the SiO_2 suspension for three time (i.e. SiO_2/GF), in which the large pores of the GF separator are completely filled with close-packed SiO_2 gel nanoparticles, and the inset shows that the SiO_2 gel nanoparticles are spherical with an average

View Article Online
DOI: 10.1039/C8TA00879E

diameter of 395 ± 55 nm (N=200). Fig.S1 in the Supporting Information illustrates the filling process of the large pores in the GF separator, where the more impregnation processing applies, and the more compact and uniform the SiO_2 gel nanoparticles are embeded. Fig.1c illustrates a smooth and poreless PU/SiO_2/GF nanocomposite separator, which was obtained after brushing the PU solution on the both sides of the SiO_2/GF separator for three times. Fig.S2 demonstrates the coating process of PU on the GF: In the beginning, the PU coating just covers a few pores among the GF fibers, and the coated region extends with the brushing times, however, there are still some parts remaining uncovered after brushing for three times, which is marked as the PU/GF separator. In contrast, Fig.S3 illustrates that the twice brushing of PU solution primarily covers the SiO_2/GF separator, and the third time brushing results in a smooth and compact PU coating, highlighting the role of the SiO_2/GF framework on constructing the PU/SiO_2/GF nanocomposite separator. To estimate the average loading amounts SiO_2 nanoparticles and PU, a group of 10 GF separators were used to prepare the SiO_2/GF and then PU/SiO_2/GF separators in sequence, and the weight differences between the SiO_2/GF and GF, and between PU/SiO_2/GF and SiO_2/GF were attributed to the contents of SiO_2 and PU. The results are listed in Table S1 in the Supporting Information, where the amounts of GF, SiO_2 and PU are determined as 0.032 g, 0.089 g and 0.034 g, respectively.

Fig.1d displays the XRD patterns of the GF, SiO_2/GF, PU/GF and PU/SiO_2/GF nanocomposite separators. The amorphous glass fibers (black line) present a broad band centered at 24.8°. The filling of SiO_2 gel nanoparticles (red line) exhibits a wide shoulder at 23.2°, similar to the amorphous silica,[31] and the coating of PU (blue line) brings with a shift of the band to the angle of 21.1°.[32] The PU/SiO_2/GF nanocomposite separator (pink line) displays a broad band located at about 23.3°, and the largest loading of SiO_2 nanoparticles is likely responsible for the peak shift in the overlain pattern of the constituents.

ATR-FTIR analysis was conducted to characterize the structure of the conventional GF, SiO_2/GF, PU/GF and PU/SiO_2/GF nanocomposite separators shown in Fig.2. The conventional GF separator (pink line) displays a symmetric

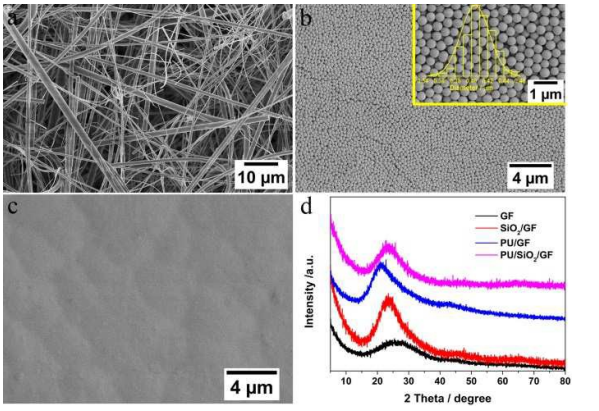

Fig.1 SEM images of the GF (a), SiO_2/GF (b) and PU/SiO_2/GF (c) separators, as well as XRD patterns of the GF, SiO_2/GF, PU/GF and PU/SiO_2/GF separators (d).

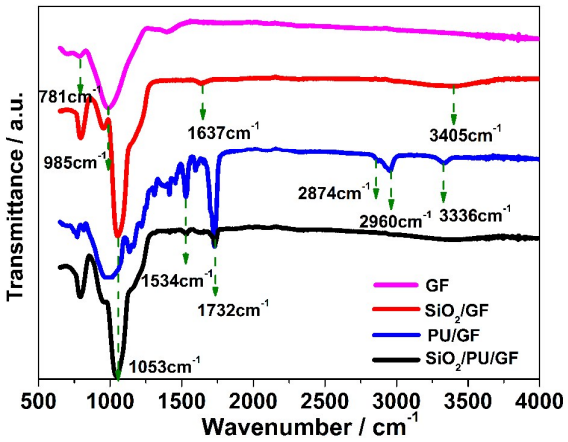

Fig.2 ATR-FTIR analysis of the GF, SiO_2/GF, PU/GF and PU/SiO_2/GF separators.

stretching vibration of Si-O at 781 cm^{-1} and an asymmetric stretching vibration of Si-O-Si at 985 cm^{-1}. After filling with SiO_2 gel nanoparticles (red line), three extra bands occur at 1053 cm^{-1}, 1637 cm^{-1} and 3405 cm^{-1} corresponding to the asymmetric stretching of Si-O-Si, bending vibration of H-O-H and O-H stretching of surface silanols, respectively.[33] The incorporation of the PU layer to GF brings with a series of new peaks (blue line), among which the peaks at 1534 cm^{-1}, 1732 cm^{-1} and 3336 cm^{-1} are attributed to the C-H stretching, C=O stretching and N-H stretching vibrations of the urethane groups, and the resonances at 2874 cm^{-1} and 2960 cm^{-1} are related to the asymmetrical and symmetric stretching vibrations of the methyl and methylene groups.[34] The PU/SiO_2/GF nanocomposite separator (black line) presents the major peaks of all the three constituents at 781 cm^{-1}, 985 cm^{-1}, 1053 cm^{-1}, 1534 cm^{-1}, 1637 cm^{-1}, 1732 cm^{-1}, 3336 cm^{-1} and 3405 cm^{-1}, respectively, demonstrating the coexistence of PU, SiO_2 gel nanoparticles and GF, in agreement with the SEM observation in Fig.1c.

Properties of the PU/SiO_2/GF nanocomposite separator

As depicted in Fig.3a, the contact angle of a water droplet on the PU/SiO_2/GF nanocomposite separator is measured as 155°, while the angle of a DMSO droplet is just 68.6°, indicating that the hydrophobic nanocomposite separator is still wettable for DMSO. Similarly, the contact angles of water and DMSO droplets on the PU/GF separator are measured as 112° and 62.5° shown in Fig.S4 in the Supporting Information, respectively. On the contrary, the water and DMSO droplets were immediately adsorbed into the conventional GF and SiO_2/GF separators (not shown), indicating that the change of surface property is assigned to the PU coating.

The water permeability of the PU/SiO_2/GF nanocomposite separator was examined by a vacuum filtration experiment following a previous article,[28] where the nanocomposite separator was employed as the filtration medium. As shown in Fig.3b, no water was observed to pass through the nanocomposite separator into the lower conical flask after 10 h, indicative of excellent water impermeability. In comparison, the GF, SiO_2/GF and PU/GF separators could not prevent from

View Article Online
DOI: 10.1039/C8TA00879E

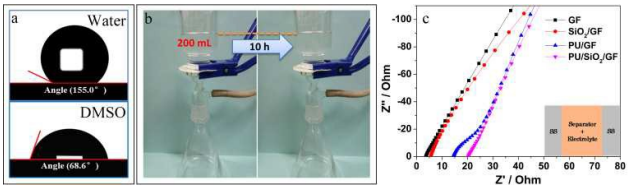

Fig.3 Contact angle measurement (a) and water permeability (b) of the PU/SiO_2/GF separator, as well as EIS analysis (c) of the GF, SiO_2/GF, PU/GF and PU/SiO_2/GF separators. Inset: Setup of the symmetric sandwich cell used for EIS analysis.

the crossover of water in the same experiment setup (not shown).

The air permeability of the conventional GF, SiO_2/GF, PU/GF and PU/SiO_2/GF nanocomposite separators was tested by a Gurley Densometer (Model 4110N, Gurley Precision Instru-ment), and the results are listed in Table 1, in which the measured Gurley times are 1.5 s, 4.5 s and 436.2 s for the GF, PU/GF and SiO_2/GF separators, respectively, suggesting that the filling of SiO_2 gel nanoparticles effectively decreases the pore size of the GF separator, while the direct coating of PU cannot fully cover the GF separator, in line with the SEM image shown in Fig.S2. Accordingly, the Gurley time of the PU/SiO_2/GF nanocomposite separator is out of range, indicative of excellent air impermeability.

The ionic conductivity (σ) of the separators was studied by electrochemical impedance spectroscopy (EIS) using a sym-metrical sandwich cell (inset of Fig.3c), where the thickness of the separator was measured by a digital micrometer. The bulk resistance R_b was read from the x-axis intercepts of the curves in the Nyquist plot (Fig.3c). As shown in Table 2, the conductivity values of the GF, SiO_2/GF, PU/GF and PU/SiO_2/GF nanocomposite separators are determined as 1.2×10^{-2} S cm^{-1}, 8.7×10^{-3} S cm^{-1}, 3.3×10^{-3} S cm^{-1} and 2.5×10^{-3} S cm^{-1}, respecttively. The conductivity of the PU/SiO_2/GF nanocompo-site separator is better than the modified Nafion (3.1×10^{-5} S cm^{-1}) and pure PU (less than 2×10^{-4} S cm^{-1}) films described in the previous reports,[28,29] which is related to the thin PU layer and the surface hydroxyl and epoxy groups on the SiO_2 gel nanoparticles, that facilitate the transfer of Li^+ across the separator.

Battery cycling with the PU/SiO_2/GF nanocomposite separator

Fig.4 demonstrates the relationship between the cycling life of Li-O_2 batteries and the structure of the separators, where the experiments were carried out in the DMSO electrolyte with 1 M $LiClO_4$ and 0.05 M LiI at fixed current density of 1 A g^{-1} and charge/discharge capacity of 1000 mAh g^{-1}. As shown in Fig.4a, the cell with the conventional GF separator displays a stable discharge platform within 60 cycles, but the terminal discharge potential declines from 2.6 V in the beginning to 2.0 V at the 60th cycle. The terminal charge potential is very low in the first cycle (3.5V), which jumps up to 4.0 V at the 10th cycle, and

Table 1 Air permeability of the separators

Sample	GF	SiO_2/GF	PU/GF	SiO_2/PU/GF
Gurley time（s）	1.5	436.2	4.5	Out of range

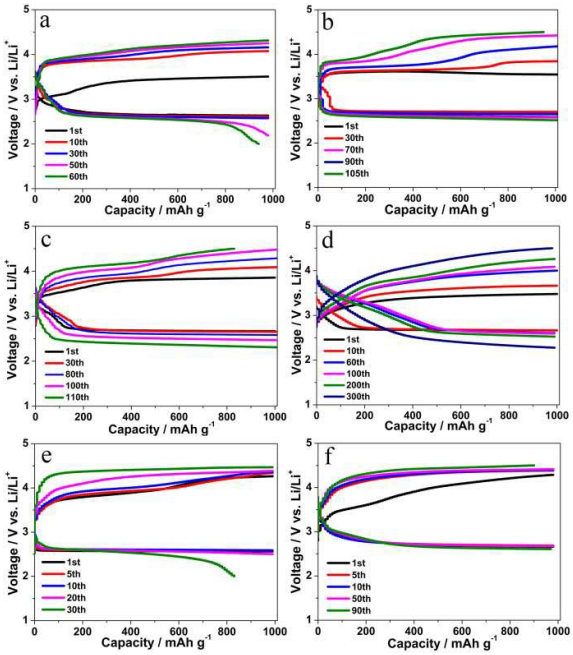

Fig.4 Voltage profiles of the Li-O_2 cells with the GF (a), SiO_2/GF (b), PU/GF (c) and PU/SiO_2/GF (d) separators with addition of 0.05 M LiI in 1 M $LiClO_4$ DMSO electrolytes, as well as the cycling curves of the cells with the GF (e) and PU/SiO_2/GF (f) separators in DMSO electrolytes with 1 M $LiClO_4$ only. The data was recorded at 1 A g^{-1} with a fixed capacity of 1000 mAh g^{-1}.

keeps on rising to 4.3 V at the 60th cycle.

Fig.4b displays stable discharge platforms within 105 cycles for the cell with the SiO_2/GF separator. The first terminal charge potential is also very low (ca. 3.5 V), which gradually climbs up to 4.5 V at the 105th cycle. The cell with PU/GF separator shown in Fig.4c exhibits a stepwise decrease on the discharge potential from 2.7 V to 2.3 V within 110 cycles, and meanwhile the terminal charge potentials are raised from 3.8 V to 4.5 V.

In comparison, the terminal discharge potential for the cell with the PU/SiO_2/GF nanocomposite separator maintains at above 2.5 V before the 200th cycle as illustrated in Fig.4d, which gradually lowers to 2.3 V at the 300th cycle. The terminal charge potential of this cell remains less than 4.3 V within the first 200 cycles, which reaches 4.5 V at 300th cycle. The testing results demonstrate that the protection of the impermeable PU/SiO_2/GF nanocomposite separator allows the Li-O_2 cells to cycle for up to 300 cycles, while those with other separators can only work no more than 110 cycles.

Fig.4e and 4f illustrate the cycling performance of the Li-O_2 batteries in the DMSO electrolytes only containing 1 M $LiClO_4$, in which the cell with the conventional GF separator can hardly

Table 2 Conductivity measurement of the separators

Sample	GF	PU/GF	SiO_2/GF	PU/SiO_2/GF
d (μm)	890	950	950	980
R_b (Ω)	3.7	14.5	5.6	20.4
σ (S cm^{-1})	1.2×10^{-2}	3.3×10^{-3}	8.7×10^{-3}	2.5×10^{-3}

View Article Online
DOI: 10.1039/C8TA00879E

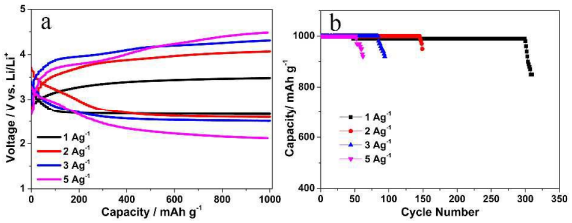

Fig.5 Rate capability (a) and cyclic performance (b) of the Li-O_2 battery at different current densities with the PU/SiO_2/GF nanocomposite separator.

run for 30 cycles, and the one with the PU/SiO_2/GF nanocomposite separator operates for 90 charge/discharge cycles, demonstrating the important role of LiI as a soluble redox mediator, which is electrochemically oxidized at the cathode interface, and in turn chemically oxidizes the insoluble Li_2O_2 to assists the decomposition of charge products in the Li-O_2 batteries.

Fig.5a illustrates the rate capability of the Li-O_2 cells with the PU/SiO_2/GF nanocomposite separator, where the potential gaps between charge plateau and discharge plateau are enlarged from 0.73 V at 1 A g^{-1} to 1.29 V, 1.62 V and 1.87 V at 2 A g^{-1}, 3 Ag^{-1} and 5 A g^{-1}, respectively. As a result, the Li-O_2 batteries can only operate properly for 146, 81 and 56 cycles at 2 A g^{-1}, 3 A g^{-1} and 5 A g^{-1} (Fig.5b), respectively.

Battery failure in presence of the PU/SiO_2/GF composite separator

The morphological change of the Li anodes after charge/discharge cycling in the Li-O_2 batteries with the conventional GF and PU/SiO_2/GF nanocomposite separators was investi-

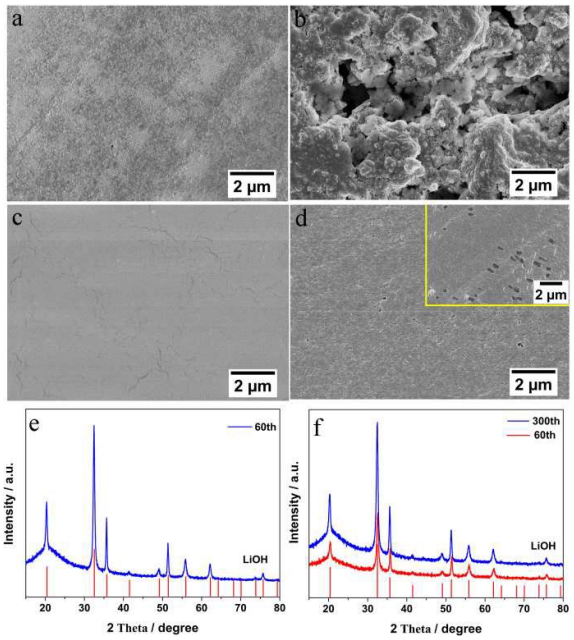

Fig.6 SEM images of pristine Li metal (a), Li anode in the cell with the GF separator after 60 cycles (b), Li anode in the cell with the PU/SiO_2/GF separator after 60 cycles (c) and 300 cycles (d, the inset shows small Li dendrites), as well as the XRD patterns of Li anodes in the cells with the GF separator after 60 cycles (e) and with the PU/SiO_2/GF separator after 60 and 300 cycles (f). Electrolyte: 0.05 M LiI and 1 M $LiClO_4$ dissolved in DMSO.

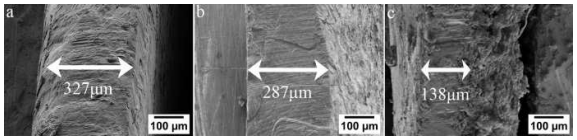

Fig.7 Cross-section SEM images of pristine Li anode (a), Li anode after 60 cycles (b) and 300 cycles (c) in the Li-O_2 battery with the PU/SiO_2/GF separator. The thickness of Li anode was measured by ImageJ software. Electrolyte: 0.05 M LiI and 1 M $LiClO_4$ dissolved in DMSO.

gated. Fig.6a illustrates the smooth surface of the Li anode prior to use. After cycling for 60 cycles, the whole Li plate in the cell with the conventional GF separator is totally eroded into white powders as shown in Fig.6b. Accordingly, the XRD pattern shown in Fig.6e displays seven major peaks at 20.4°, 32.5°, 35.7°, 51.4°, 55.9°, 62.1° and 75.8°, assigned to the (001), (101), (110), (200), (201), (211) and (113) facets of LiOH crystal (JPDF No. 85-1064), respectively, in line with the previous reports.[25,28] In comparison, the Li anode in the cell with the PU/SiO_2/GF nanocomposite separator just exhibits some tiny cracks on its smooth surface after 60 cycles as displayed in Fig.6c, and after cycling for 300 times the Li metal still exists as shown in the SEM micrograph in Fig.6d, where some pores are observed accompanied with small dendrites (inset of Fig.6d), different from the large and long dendrites frequently reported in previous literature.[28,35]

Fig.6f presents the XRD pattern of the powders collected from the Li anode, which exhibits seven major peaks at 20.3°, 32.5°, 35.7°, 51.4°, 55.8°, 62.2° and 75.6°, ascribed to the (001), (101), (110), (200), (201), (211), and (113) facets of LiOH crystal (JPDF No. 85-1064), respectively, and the intensity of the peaks in Fig.6f increases with cycling times, demonstrating that heavier corrosion happened on the Li anode as more charge/discharge cycles were applied, which resulted in the accumulation of LiOH on the surface, in line with previous literature.[36]

The anode thickness in the cells with the GF, SiO_2/GF, PU/GF and PU/SiO_2/GF separators were also examined with cycling. The average thickness of the pristine Li plate is 327 μm shown in Fig.7a, which becomes 181 μm with a rough surface only after 30 cycles with the GF separator (shown in Fig.S5a and S5d in the Supporting Information), and at the 55th cycle the Li is totally consumed. In comparison, the residual thickness of Li plate at 60th cycle is determined as 204 μm for the SiO_2/GF separator (Fig.S5b and S5e), 176μm for the PU/GF separator (Fig.S5c and S5f), and 287μm for the PU/SiO_2/GF separator (Fig.7b), demonstrating the Li decay is in an order of GF>PU/GF>SiO_2/GF>PU/SiO_2/GF. Moreover, the Li plate can still remain up to 138 μm (Fig.7c) after cycling for 300 times for the PU/SiO_2/GF separator, i.e. about 42% of Li metal is kept.

Fig.8 illustrates the SEM micrographs of the MWNTs cathode during charge/discharge cycling. Compared with the pristine MWNTs (Fig.8a), the MWNTs cathode in the cell with the conventional GF separator is seriously blocked up only after 60 charge/discharge cycles (Fig.8b). In contrast, the 60 cycles just results in a thin layer of discharge product on the MWNTs cathode by using the PU/SiO_2/GF nanocomposite

View Article Online
DOI: 10.1039/C8TA00879E

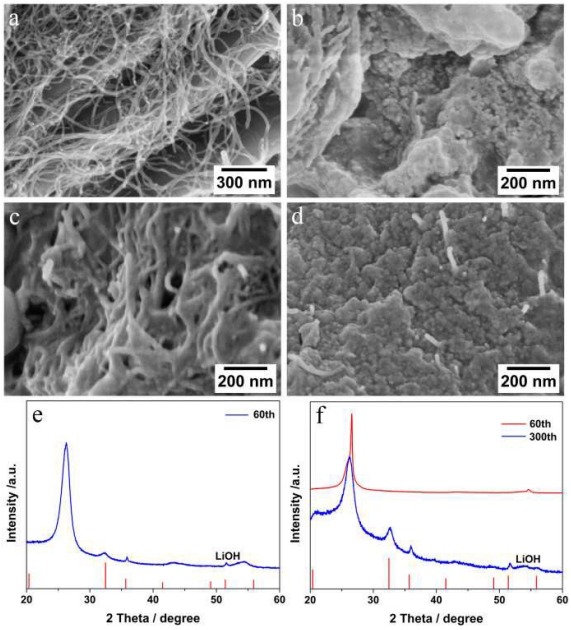

Fig.8 SEM micrographs of MWNTs cathode prior to use (a), MWNTs cathode after 60 cycles in the cell with GF separator (b), MWNTs cathode after 60 (c) and 300 cycles (d) in the cell with the PU/SiO_2/GF separator, as well as the XRD patterns of the MWNTs cathode in the cells with the GF separator after 60 cycles (e) and with the PU/SiO_2/GF separator after 60 and 300 cycles (f), respectively. Electrolyte: 0.05 M LiI and 1 M $LiClO_4$ dissolved in DMSO.

separator (Fig.8c), however, at the 300th cycle the solid product basically clogs the pores of the MWNTs cathode (Fig.8d), suggesting that the passivation of the MWNTs cathode is responsible for the failure of the Li-O_2 batteries with the PU/SiO_2/GF nanocomposite separator, because the Li anode is still available for battery reaction as shown in Fig.7c.

The XRD analysis of the MWNTs cathode in the cell with the GF separator (Fig.8e) exhibits three peaks at about 32.7°, 35.9° and 51.7° after 60 cycles, which are attributed to the (101), (110) and (200) facets of LiOH crystal (JPDF No. 85-1064). For the one with the and PU/SiO_2/GF nanocomposite separator (Fig.8f), no XRD signals attributed to LiOH are seen at the 60th cycle, but at the 300th cycle three peaks at about 32.7°, 35.9° and 51.7° appear, attributed to the (101), (110) and (200) facets of LiOH crystal (JPDF No. 85-1064), respectively, indicating that more charge/discharge cycles are required for product accumulation in the presence of the PU/SiO_2/GF nanocomposite separator. The result identifies again the necessity of using LiI in the experiment,[13] in agreement with the battery testing in Fig.4.

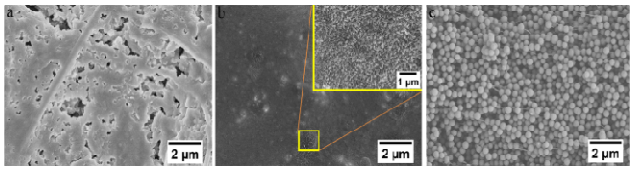

Fig.9 SEM images of the GF separator after 60 cycles (a), and the PU/SiO_2/GF separator after 60 cycles (b) and 300 cycles (c). Electrolyte: 0.05 M LiI and 1 M $LiClO_4$ dissolved in DMSO.

Fig.9 illustrates the morphological evolution of the battery separators after long-term cycling. It is noticed that the conventional GF separator is filled with the discharge product after cycling for 60 times (Fig.9a), indicative of the immigration of soluble oxidative species toward the Li anode, that react to precipitate in the midway. In contrast, the PU/SiO_2/GF nanocomposite separator remains clean after 60 cycles (Fig.9b), although the PU coating at some parts of the separator has been decomposed by soluble oxidative intermediates by oxygen reduction reaction (inset of Fig.9b). After 300 cycles, the PU coating of the PU/SiO_2/GF nanocomposite separator is basically decomposed (Fig.9c), but the surface of the separator still keeps clear of any precipitates.

The above results suggest that the PU/SiO_2/GF nanocomposite separator exerts important effect on the protection of Li anode, owing to the resistance to the crossover of the soluble oxidative species by the dense molecular networks of the PU layer. Therefore, the cycling life of the Li-O_2 battery actually relies heavily on the effective decomposition of the discharge product on the MWNTs cathode in the presence of the PU/SiO_2/GF nanocomposite separator, which is different from the one using the conventional GF separator.

Conclusion

The cycling performance of aprotic Li-O_2 batteries was significantly enhanced by using the PU/SiO_2/GF nanocomposite separator, where the SiO_2 gel nanoparticles served to fill the large pores of the conventional GF separator and conduct Li^+ across the separator, and the outer PU coating sealed the separator to be water and air impermeable by its dense molecular network. The Li anode was effectively protected in the presence of the nanocomposite separator, where 42% of Li metal remained after 300 charge/discharge cycles at the persistent capacity of 1000 mAh g^{-1}, in comparison to the maximum 60 cycles for the cell with the conventional GF separator. The PU layer of the nanocomposite separator was gradually decomposed by oxidative intermediates generated by ORR, but the battery failure in presence of the PU/SiO_2/GF nanocomposite separator is still attributed to the passivation of cathode instead of Li anode consumption. Effective methods to promote the decomposition of discharge products are currently under development.

Acknowledgements

This work was supported by Guangxi Natural Science Foundation (No. 2015GXNSFBA139220 and 2016GXNSFAA380107) and the funding from the Collaborative Innovation Center for Exploration of Hidden Nonferrous Metal Deposits & Development of New Materials in Guangxi, and Guangxi Key Laboratory of Universities for Clean Metallurgy Comprehensive Utilization of Nonferrous Metal Resource. K. L. greatly appre-

View Article Online
DOI: 10.1039/C8TA00879E

ciates the assistance from Dr. Pierrot Attidekou and Dr. Mohamed Mamlouk on battery assembly in glovebox and battery testing during his visit in the Newcastle University.

Notes and references

1 F. J. Li, T. Zhang and H. S. Zhou, Energy Environ. Sci., 2013, **6**, 1125-1141.
2 Z. Peng, S. A. Freunberger, Y. Chen and P. G. Bruce, Science, 2012, **337**, 563-566.
3 X. W. Guo, P. Liu, J. H. Han, Y. Ito, A. Hirata, T. Fujita and M. W. Chen, Adv. Mater., 2015, **27**, 6137-6143.
4 J. L. Shui, F. Du, C. M. Xue, Q. Li and L. M. Dai, ACS Nano, 2014, **8**, 3015-3022.
5 H. D. Lim, H. Song, J. Kim, H. Gwon, Y. Bae, K. Y. Park, J. Hong, H. Kim, T. Kim, Y. H. Kim, X. Lepro, R. Ovallerobles, R. H. Baughman and K. Kang, Angew. Chem. Int. Ed., 2014, **126**, 4007-4012.
6 B. J. Bergner, A. Schürmann, K. Peppler, A. Garsuch and J. Janek, J. Am. Chem. Soc., 2014, **136**, 15054-15064.
7 Y. Chen, S. A. Freunberger, Z. Peng, O. Fontaine and P. G. Bruce, Nat. Chem., 2013, **5**, 489-494.
8 D. Sun, Y. Shen, W. Zhang, L. Yu and Z. Yi, J. Am. Chem. Soc., 2014, **136**, 8941-8946.
9 L. Johnson, C. M. Li, Z. Liu, Y. H. Chen, S. A. Freunberger, J. M. Tarascon, P. C. Ashok, B. B. Praveen, K. Dholakia and P. G. Bruce, Nat. Chem., 2014, **6**, 1091-1099.
10 J. J. Xu, Z. W. Chang, Y. Wang, D. P. Liu, Y. Zhang and X. B. Zhang, Adv. Mater., 2016, **28**, 9620-9628.
11 L. D. Griffith, A. Sleightholme, J. F. Mansfield, D. J. Siegel and C. W. Monroe, ACS Appl. Mater. Interfaces, 2015, **7**, 7670-7678.
12 J. Lu, Y. J. Lee, X. Y. Luo, K. C. Lau, M. Asadi, H. H. Wang, S. Brombosz, J. G. Wen, D. Y. Zhai, Z. G. Chen, D. J. Miller, Y. S. Jeong, J. B. Park, Z. Z. Fang, B. Kumar, A. Salehi-Khojin, Y. K. Sun, L. A. Curtiss and K. Amine, Nature, 2016, **529**, 377-382.
13 T. Liu, M. Leskes, W. J. Yu, A. J. Moore, L. N. Zhou, P. M. Bayley, G. Kim and C. P Grey, Science, 2015, **350**,530-533.
14 Y. Qiao, S. C. Wu, J. Yi, Y. Sun, S. H. Guo, S. X. Yang, P. He and H. S. Zhou, Angew. Chem. Int. Ed., 2017, **56**, 4960-4964.
15 D. C. Lin, Y. Y. Liu and Y. Cui, Nat. Nanotech., 2017, **12**, 194-206.
16 Y. P. Guo, H. Q. Li and T. Y. Zhai, Adv. Mater., 2017, **29**, 1700007.
17 N. N. Feng, P. He and H. S. Zhou, Adv. Energy Mater., 2016, **6**, 1502303.
18 R. S. Assary, J. Lu, P. Du, X. Y. Luo, X. Y. Zhang, Y. Ren, L. A. Curtiss and K. Amine, ChemSusChem., 2013, **6**, 51-55.
19 E. Nasybulin, W. Xu, M. H. Engelhard, Z. Nie, X. S. Li and J. G. Zhang, J. Power Sources, 2013, **243**, 899-907.
20 B. Liu, W. Xu, P. F. Yan, X. L. Sun, M. E. Bowden, J. Read, J. F. Qian, D. H. Mei, C. M. Wang and J. G. Zhang, Adv. Funct. Mater., 2016, **26**, 605-613.
21 W. J. Kwak, D. Hirshberg, D. Sharon, H. J Shin, M. Afri, J. B. Park, A. Garsuch, F. F. Chesneau, A. A. Frimer, D. Aurbach and Y. K. Sun, J. Mater. Chem. A, 2015, **3**, 8855-8864.
22 J. Hassoun, H. G. Jung, D. J. Lee, J. B. Park, K. Amine, Y. K. Sun and B. Scrosati, Nano Lett., 2012, **12**, 5775-5779.
23 Z. Y. Guo, X. L. Dong, Y. G. Wang and Y. Y. Xia, Chem. Commun., 2015, **51**, 676-678.
24 T. Zhang, K. M. Liao, P. He and H. S. Zhou, Energy Environ. Sci., 2016, **9**, 1024-1030.
25 Q. C. Liu, J. J. Xu, S. Yuan, Z. W. Chang, D. Xu, Y. B. Yin, L. Li, H. X. Zhong, Y. S. Jiang, J. M. Yan and X. B. Zhang, Adv. Mater., 2015, **27**, 5241-5247.
26 D. J. Lee, H. Lee, Y. J. Kim, J. K. Park and H. T. Kim, Adv. Mater., 2016, **28**, 857-863.
27 J. H. Kim, H. S. Woo, W. K. Kim, K. H. Ryu and D. W. Kim, ACS Appl. Mater. Interfaces, 2016, **8**, 32300-32306.
28 B. G. Kim, J. S. Kim, J. Min, Y. H. Lee, J. H. Choi, M. C. Jang, S. A. Freunberger and J. W. Choi, Adv. Funct. Mater., 2016, **26**, 1747-1756.
29 J. J. Xu, Q. C. Liu, Y. Yu, J. Wang, J. M. Yan and X. B. Zhang, Adv. Mater., 2017, **29**, 1606552.
30 M. Bardosova and R. H. Tredgold, J. Mater. Chem., 2002, **12**, 2835-2842.
31 X. H. Yu, Z. Zhao, Y. C. Wei, J. Liu, J. M. Li, A. J. Duan and G. Y. Jiang, RSC Adv., 2015, **5**, 49780-49790.
32 N. Lin, S. W. Wei, T. Xia, F. Hu, J. Huang and A. Dufresne, RSC Adv., 2014, **4**, 49098-49107.
33 V. G. Pol, S. V. Pol, P. P. George, B. Markovsky and A. Gedanken, J. Phys. Chem. B, 2006, **110**, 13420-13424.
34 C. C. Xu, Y. H. Huang, L. P. Tang and Y. Hong, ACS Appl. Mater. Interfaces, 2017, **9**, 2169-2180.
35 J. S. Kim, T. H. Hwang, B. G. Kim, J. Min and J. W. Choi, Adv. Funct. Mater., 2014, **24**, 5359-5367.
36 J. L. Shui, J. S. Okasinski, P. Kenesei, H. A. Dobbs, D. Zhao, J. D. Almer and D. J. Liu, Nat. Commun., 2013, **4**, 2255-2262.

View Article Online
DOI: 10.1039/C8TA00879E

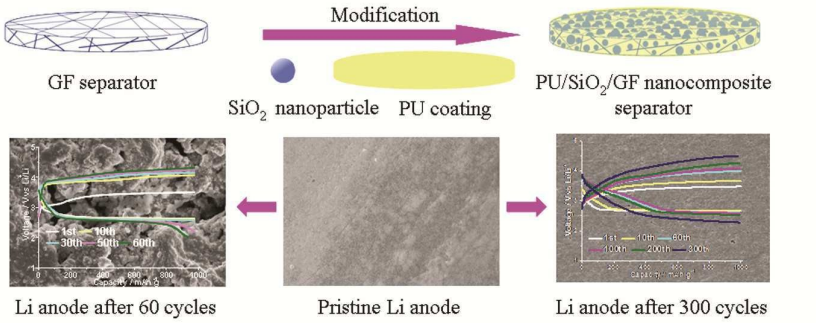

The cyclic performance of Li-O_2 batteries is significantly enhanced by using the PU/SiO_2/GF nanocomposite separator, which effectively protects Li anode from corrosion by soluble oxidative intermediates from ORR, and the dendritic growth of Li crystal during cycling is also inhibited.